JOURNAL OF COMPUTATIONAL PHYSICS 13, 181–208 (1973)

Alternating Direction Implicit Techniques for Two-Dimensional Magnetohydrodynamic Calculations

IRVIN LINDEMUTH

Lawrence Livermore Laboratory, Livermore, California 94550

AND

JOHN KILLEEN

Lawrence Livermore Laboratory, Livermore, California 94550
and
Department of Applied Science, University of California/Davis, Livermore, California 94550

Received March 16, 1973

Alternating direction implicit numerical techniques for solving time-dependent, two-dimensional, two-fluid magnetohydrodynamic equations are presented. The techniques are illustrated with applications to the dynamics of a theta pinch and the expansion of a laser produced plasma and important features of both cases are demonstrated. The enhanced numerical stability of the method is discussed.

INTRODUCTION

The rapid advance in computer technology in recent years has led to an effort to extend the state of the art in computational magnetohydrodynamics to two dimensions. The pioneering work of Hain *et al.* [1] in one-dimensional calculations occurred just over a decade ago and has been developed and extended to the point where Roberts and Potter [2], in their recent review of magnetohydrodynamic calculations, have suggested that presently realistic one-dimensional calculations are routine. The theta pinch computations of Duchs [3] are the first two-dimensional calculations using a reasonably complete model to be published. Freeman and Lane [4] presented some theta pinch results, and their code has recently been applied to the study of the interaction of a plasmoid with a solenoidal magnetic field [5]. The plasma focus calculations by Potter [6] have been presented in the review of Roberts and Potter [2]. Hertweck and Schneider [7], and more recently

Schneider [8], have performed computations on the dynamics of a theta pinch. Chase, LeBlanc, and Wilson have used a two-dimensional magnetohydrodynamic model to investigate the role of spontaneous magnetic fields in a laser-produced plasma [9]. With the exception of the work of Hertweck and Schneider, all of the calculations have been of the Eulerian type. In Hertweck and Schneider's work the grid lines are the magnetic field lines, but the work is limited by an assumption of infinite conductivity.

The magnetohydrodynamic models used are similar and are various approximations to the more complete model given by Braginskii [10]. The models have as characteristic velocities the fluid velocity and magnetosonic velocity and include thermal diffusion of energy and resistive diffusion of the magnetic field. The requirement for numerical stability of an explicit scheme leads to an upper bound on the time step Δt given by $\Delta t \leqslant v\,\Delta x$, where v is the maximum characteristic velocity, and Δx is a spatial zone size, or $\Delta t \leqslant k(\Delta x)^2/2$, where k is the maximum diffusion coefficient. The restrictions are, of course, conditions which must be satisfied throughout the entire grid, and often the lowest upper bound occurs in a region which is not the most important region from a physical standpoint. Because the quadratic dependence of the second condition quite often leads to a severe restriction on the time step, several authors cited above have incorporated the alternating direction implicit (ADI) method of Peaceman and Rachford [11] into their finite difference schemes. Others use "splitting" and an implicit scheme to handle the thermal and resistive diffusion. However, even those who have implemented such procedures retain an explicit treatment of convective transport.

In this paper, a method for calculating simultaneously both convective and diffusive two-dimensional transport in magnetohydrodynamics using alternating direction implicit finite difference equations is presented. The rationale for this work is, of course, that alternating direction implicit equations allow information to propagate from a grid point to any other point in the finite difference mesh within two time steps, so that time step restrictions, if any, should not be as severe as those encountered with explicit methods.

As applications of the method, calculations demonstrating the dynamics of a theta pinch in a mirror magnetic field and the expansion of a high density plasma sphere (e.g., a laser-produced plasma) into a uniform magnetic field are included.

Magnetohydrodynamic Model

We use a two-fluid model, i.e., separate temperatures are calculated for ions and electrons. The pressure is a scalar, but the thermal conductivity and electrical resistivity are tensors. The equations solved are given by

$$(\partial\rho/\partial t) + \mathbf{v}\cdot\nabla\rho + \rho\nabla\cdot\mathbf{v} = 0, \tag{1}$$

$$\frac{\partial\mathbf{v}}{\partial t} + \mathbf{v}\cdot\nabla\mathbf{v} + \nabla(\theta_i + \theta_e) + \frac{\theta_i + \theta_e}{\rho}\nabla\rho + \frac{1}{\rho\mu_0}\mathbf{B}\times(\nabla\times\mathbf{B}) = 0; \tag{2}$$

$$\frac{\partial\theta_i}{\partial t} + \mathbf{v}\cdot\nabla\theta_i + (\gamma-1)\,\theta_i\nabla\cdot\mathbf{v} - \frac{1}{\rho}\nabla\cdot(\overline{K}_i\cdot\nabla\theta_i) + f_{eq}(\theta_i - \theta_e) = 0; \tag{3}$$

$$\frac{\partial\theta_e}{\partial t} + \mathbf{v}\cdot\nabla\theta_e + (\gamma-1)\,\theta_e\nabla\cdot\mathbf{v} - \frac{1}{\rho}\nabla\cdot(\overline{K}_e\cdot\nabla\theta_e) + f_{eq}(\theta_e - \theta_i) - \frac{(\gamma-1)}{\rho\mu_0{}^2}(\bar{\bar{\eta}}\cdot\nabla\times\mathbf{B})\cdot(\nabla\times\mathbf{B}) = 0; \tag{4}$$

$$(\partial\mathbf{B}/\partial t) + \mathbf{v}\cdot\nabla\mathbf{B} + \mathbf{B}(\nabla\cdot\mathbf{v}) - \mathbf{B}\cdot\nabla\mathbf{v} + (1/\mu_0)\,\nabla\times(\bar{\bar{\eta}}\cdot\nabla\times\mathbf{B}) = 0; \tag{5}$$

where ρ is the mass density, $\mathbf{v}$ the fluid velocity, θ_e and θ_i the electron and ion temperatures, and $\mathbf{B}$ the magnetic field; the transport coefficients f_{eq}, $\bar{\bar{\eta}}$, $\overline{K}_i$, and $\overline{K}_e$ are the equipartition frequency, resistivity matrix, ion thermal conductivity matrix and electron thermal conductivity matrix, respectively, and γ, μ_0 are constants.

The use of tensor thermal conductivities and tensor resistivity implies the presence of a magnetic field which, although not strong enough to lead to anisotropic temperatures, is strong enough to alter the thermal conduction and resistance in directions perpendicular to the magnetic field. The heat flow vector $\mathbf{q}_\alpha$ is given by

$$(\mathbf{q}_\alpha)_\perp = -(K_\alpha)_\perp(\nabla\theta_\alpha)_\perp - \{(K_\alpha)_\perp[(K_\alpha)_\parallel - (K_\alpha)_\perp]\}^{1/2}((\mathbf{B}\times\nabla\theta_\alpha)/B) \tag{6}$$

and

$$(\mathbf{q}_\alpha)_\parallel = -(K_\alpha)_\parallel(\nabla\theta_\alpha)_\parallel . \tag{7}$$

In Eqs. (6) and (7) the subscript symbols $\perp$ and $\parallel$ are used to designate components of vectors perpendicular and parallel, respectively to the magnetic field and to differentiate between perpendicular and parallel transport coefficients.

The transport coefficients used in the calculations shown in this paper were taken from Spitzer [12] and Kaufman [13]. Spitzer's equipartition frequency, strong field resistivity, and parallel thermal conductivities, including the factors ϵ and δ_T, have been used. Kaufman's strong field thermal conductivities, with Spitzer's Coulomb logarithm, have been used with the interpolation method of Hain *et al.* [1] to calculate the perpendicular thermal conductivities. We emphasize, however, that the numerical method reported here does not depend on the specific form of the coefficients and the computer code in which the method has been implemented has been purposely set up to facilitate using forms other than those actually used in the calculations of this article.

The equations describe the temporal and spatial variation of nine quantities, the density, the three velocity components, the ion and electron temperature, and the three magnetic-field components. It is convenient to introduce a vector **U** which has as its components all the dependent variables to be calculated, and a vector **K** which has as its components all the transport coefficients, so that for the complete set of two-fluid equations, in two dimensions, the vectors are

$$\mathbf{U} = \mathbf{U}(r, z, t) = (\rho, v_r, v_\varnothing, v_z, \theta_i, \theta_e, B_r, B_\varnothing, B_z) \tag{8}$$

and

$$\mathbf{K} = \mathbf{K}(\mathbf{U}) = (K_i^{rr}, K_i^{zz}, K_i^{rz}, K_i^{zr}, K_e^{rr}, K_e^{zz}, K_e^{rz}, K_e^{zr}, f_{eq}, \eta_{rr}, \eta_{rz}, \eta_{r\varnothing}, \eta_{\varnothing\varnothing}, \eta_{\varnothing z}, \eta_{zz}), \tag{9}$$

where the superscripts have been used for convenience to designate components of the thermal conductivity matrices.

It is possible to write the equations in a variety of ways, all of which in differential form are exactly equivalent; in many cases, a "conservative" form of the differential equations in which derivatives are not expanded leads to the best finite difference equations. It is also possible to introduce alternate variables. For example, the specific volume $V = 1/\rho$ and the pressures $P_\alpha = \rho\theta_\alpha$ are often calculated in computational hydrodynamics. For any magnetohydrodynamic model in which B_r and B_z are to be calculated, it is advantageous to calculate directly a stream function ψ given by

$$\psi = rA_\varnothing . \tag{10}$$

Both B_r and B_z can be calculated from ψ as

$$B_r = -(1/r)(\partial\psi/\partial z) \qquad B_z = (1/r)(\partial\psi/\partial r). \tag{11}$$

The introduction of ψ as an alternate variable has the advantage of reducing by one the number of equations to be solved and also facilitates the determination of magnetic field lines, which are the contours of constant ψ, and also guarantees that div $\mathbf{B} = 0$.

Difference Methods

It is possible to consider varied explicit finite difference approximations to the two-dimensional magnetohydrodynamic partial differential equations. When one then considers implicit or alternating direction implicit approximations, the number of possibilities increases. Consequently, in the course of development of the

method given here, many schemes have been excluded, some rather arbitrarily. In this section, the basic features of the method which have persisted are presented. In essence, the method is Eulerian, linear, two level, and simultaneous.

The finite difference equations are purposely intended to be linear in the dependent variables at the new time step, and, in fact, it is the linearization which is a fundamental feature of the method. In contrast to explicit difference equations, the linear ADI difference equations given here are coupled in all unknown dependent variables, both at a particular mesh point and its adjacent neighboring mesh points.

The finite difference equations are written in terms of quantities at only two time levels. The basic structure of the original work of Peaceman and Rachford [11] is retained in that two different finite difference approximations are used alternately, one to advance the calculations from a time t^n to a time t^{n+1} and a second from t^{n+1} to t^{n+2}, and the second approximation needs no information about the values at t^n. The bilevel equations have obvious advantages in requiring minimal memory size and in facilitating time step variation; the time step can be varied after each two time steps with no loss in truncation error. In conjunction with the bilevel equations, a nonstaggered spatial array is used so that all dependent variables are defined at the same spacetime point.

Finally, a very important property of the method is that all physical processes are calculated simultaneously. With only one sweep through the mesh with either of the alternately used difference approximations, all convective, diffusive, and local processes are calculated directly without the need to calculate intermediate values.

The set of partial differential equations to be solved can be written as

$$\frac{\partial \mathbf{U}}{\partial t} + \mathbf{T}\left(\mathbf{U}, \frac{\partial \mathbf{U}}{\partial r}, \frac{\partial \mathbf{U}}{\partial z}, \frac{\partial^2 \mathbf{U}}{\partial r^2}, \frac{\partial^2 \mathbf{U}}{\partial z^2}, \mathbf{K}, \frac{\partial \mathbf{K}}{\partial r}, \frac{\partial \mathbf{K}}{\partial z}\right) = 0, \tag{12}$$

where $\mathbf{T}$ is a vector function of the arguments indicated. (We consider the case of mixed derivatives later.)

In the following, a superscript n and subscripts i and j will refer to the point (t^n, r_i, z_j) in the spacetime mesh.

Equation (12) states that

$$(\partial \mathbf{U}/\partial t)_{i,j}^{n+1} + \mathbf{T}_{i,j}^{n+1} = 0. \tag{13}$$

The β component of $\mathbf{T}$ can be written as

$$T_\beta = \mathbf{f}^\beta\left(\mathbf{U}, \frac{\partial \mathbf{U}}{\partial r}, \frac{\partial^2 \mathbf{U}}{\partial r^2}, \mathbf{K}, \frac{\partial \mathbf{K}}{\partial r}\right) \cdot \mathbf{g}^\beta\left(\mathbf{U}, \frac{\partial \mathbf{U}}{\partial z}, \frac{\partial^2 \mathbf{U}}{\partial z^2}, \mathbf{K}, \frac{\partial \mathbf{K}}{\partial z}\right), \tag{14}$$

where $\mathbf{f}^\beta$ and $\mathbf{g}^\beta$ are vector functions of the arguments indicated. The problem now is to put $\mathbf{f}^\beta$ and $\mathbf{g}^\beta$ into useful forms. This can be accomplished correct to second order in Δt by using a linearization procedure. A Taylor expansion of the ϵ component of $\mathbf{f}^\beta$ gives

$$(f_\epsilon^\beta)_{i,j}^{n+1} = f_\epsilon^\beta + \Delta t \left\{ \left[\frac{\partial f_\epsilon^\beta}{\partial U_\alpha} + \frac{\partial f_\epsilon^\beta}{\partial K_\gamma} \frac{\partial K_\gamma}{\partial U_\alpha} + \frac{\partial f_\epsilon^\beta}{\partial (\partial K_\gamma/\partial r)} \frac{\partial^2 K_\gamma}{\partial U_\alpha \, \partial r} \right] \frac{\partial U_\alpha}{\partial t} \right.$$

$$\left. + \left[\frac{\partial f_\epsilon^\beta}{\partial (\partial U_\alpha/\partial r)} + \frac{\partial f_\epsilon^\beta}{\partial (\partial K_\gamma/\partial r)} \frac{\partial K_\gamma}{\partial U_\alpha} \right] \frac{\partial^2 U_\alpha}{\partial r \, \partial t} + \frac{\partial f_\epsilon^\beta}{\partial (\partial^2 U_\alpha/\partial r^2)} \frac{\partial^3 U_\alpha}{\partial r^2 \, \partial t} \right\}, \quad (15)$$

where the superscript n and the subscripts i and j are expressly implied for all quantities on the right-hand side, and where repeated subscripts α and γ imply a summation. Replacing the time derivatives by forward differences, we can write the first approximation to Eq. (13) as

$$(\bar{A}')_{i,j}^n \, \mathbf{U}_{i,j}^{n+1} + (\bar{B}')_{i,j}^n (\partial \mathbf{U}/\partial r)_{i,j}^{n+1} + (\bar{C}')_{i,j}^n (\partial^2 \mathbf{U}/\partial r^2)_{i,j}^{n+1} = (\mathbf{V}')_{i,j}^n , \quad (16)$$

where $\bar{A}'$, $\bar{B}'$, and $\bar{C}'$ are matrices, functionally dependent on $\mathbf{U}$, $\partial \mathbf{U}/\partial r$, $\partial^2 \mathbf{U}/\partial r^2$, $\mathbf{K}$, $\partial \mathbf{K}/\partial r$, $\partial \mathbf{U}/\partial z$, $\partial^2 \mathbf{U}/\partial z^2$, and $\partial \mathbf{K}/\partial z$, and having elements

$$A'_{\beta\alpha} = \frac{\delta_{\beta\alpha}}{\Delta t} + g_\epsilon^\beta \left[\frac{\partial f_\epsilon^\beta}{\partial U_\alpha} + \frac{\partial f_\epsilon^\beta}{\partial K_\gamma} \frac{\partial K_\gamma}{\partial U_\alpha} + \frac{\partial f_\epsilon^\beta}{\partial (\partial K_\gamma/\partial r)} \frac{\partial^2 K_\gamma}{\partial U_\alpha \, \partial r} \right], \quad (17)$$

$$B'_{\beta\alpha} = g_\epsilon^\beta \left[\frac{\partial f_\epsilon^\beta}{\partial (\partial U_\alpha/\partial r)} + \frac{\partial f_\epsilon^\beta}{\partial (\partial K_\gamma/\partial r)} \frac{\partial K_\gamma}{\partial U_\alpha} \right], \quad (18)$$

$$C'_{\beta\alpha} = g_\epsilon^\beta \, \partial f_\epsilon^\beta / \partial (\partial^2 U_\alpha/\partial r^2), \quad (19)$$

and $\mathbf{V}'$ is a vector with components

$$V_\beta' = -g_\epsilon^\beta f_\epsilon^\beta + A'_{\beta\alpha} U_\alpha + B'_{\beta\alpha} (\partial U_\alpha/\partial r) + C'_{\beta\alpha} (\partial^2 U_\alpha/\partial r^2). \quad (20)$$

In Eqs. (17) through (20), the superscripts n and subscripts i and j are expressly implied, and the repeated subscripts α, γ, and ϵ indicate a summation, but no summation is indicated by the repeated superscript β on g and f. The Kronecker delta $\delta_{\beta\alpha}$, appears in Eq. (17). Defining $(\Delta r_+)_i = r_{i+1} - r_i$ and $(\Delta r_-)_i = r_i - r_{i-1}$, one can put Eq. (16) into its final form,

$$(\bar{A})_{i,j}^n \, \mathbf{U}_{i,j}^{n+1} + (\bar{B})_{i,j}^n \, \mathbf{U}_{i+1,j}^{n+1} - (\bar{C})_{i,j}^n \, \mathbf{U}_{i-1,j}^{n+1} = \mathbf{V}_{i,j}^n , \quad (21)$$

with

$$A_{\beta\alpha} = A'_{\beta\alpha} + \frac{\Delta r_+ - \Delta r_-}{\Delta r_+ \Delta r_-} B'_{\beta\alpha} - \frac{2}{\Delta r_+ \Delta r_-} C'_{\beta\alpha}, \tag{22}$$

$$B_{\beta\alpha} = \frac{\Delta r_-}{\Delta r_+(\Delta r_- + \Delta r_+)} B'_{\beta\alpha} + \frac{2}{\Delta r_+(\Delta r_- + \Delta r_+)} C'_{\beta\alpha}, \tag{23}$$

$$C_{\beta\alpha} = \frac{\Delta r_+}{\Delta r_-(\Delta r_- + \Delta r_+)} B'_{\beta\alpha} - \frac{2}{\Delta r_-(\Delta r_- + \Delta r_+)} C'_{\beta\alpha} \tag{24}$$

and

$$V_\beta = V_\beta'. \tag{25}$$

Analogous to Eq. (15), a Taylor expansion of the ϵ component of $\mathbf{g}^\beta$ gives

$$(g_\epsilon^\beta)_{i,j}^{n+2} = g_\epsilon^\beta + \Delta t \left\{ \left[\frac{\partial g_\epsilon^\beta}{\partial U_\alpha} + \frac{\partial g_\epsilon^\beta}{\partial K_\gamma} \frac{\partial K_\gamma}{\partial U_\alpha} + \frac{\partial g_\epsilon^\beta}{\partial(\partial K_\gamma/\partial z)} \frac{\partial^2 K_\gamma}{\partial U_\alpha \partial z} \right] \frac{\partial U_\alpha}{\partial t} \right.$$
$$\left. + \left[\frac{\partial g_\epsilon^\beta}{\partial(\partial U_\alpha/\partial z)} + \frac{\partial g_\epsilon^\beta}{\partial(\partial K_\gamma/\partial z)} \frac{\partial K_\gamma}{\partial U_\alpha} \right] \frac{\partial^2 U_\alpha}{\partial z \, \partial t} + \frac{\partial g_\epsilon^\beta}{\partial(\partial^2 U_\alpha/\partial z^2)} \frac{\partial^3 U}{\partial z^2 \, \partial t} \right\}, \tag{26}$$

where here a superscript $n + 1$ as well as subscripts i and j are expressly implied for all quantities on the right-hand side. Then we can write the second approximation to (13) as

$$(\bar{A}')_{i,j}^{n+1} \mathbf{U}_{i,j}^{n+2} + (\bar{B}')_{i,j}^{n+1} (\partial \mathbf{U}/\partial z)_{i,j}^{n+2} + (\bar{C}')_{i,j}^{n+1} (\partial^2 \mathbf{U}/\partial z^2)_{i,j}^{n+2} = (\mathbf{V}')_{i,j}^{n+1}, \tag{27}$$

where $\bar{A}'$, $\bar{B}'$, $\bar{C}'$, and $\mathbf{V}'$ are given by

$$A'_{\beta\alpha} = \frac{\delta_{\beta\alpha}}{\Delta t} + f_\epsilon^\beta \left[\frac{\partial g_\epsilon^\beta}{\partial U_\alpha} + \frac{\partial g_\epsilon^\beta}{\partial K_\gamma} \frac{\partial K_\gamma}{\partial U_\alpha} + \frac{\partial g_\epsilon^\beta}{\partial(\partial K_\gamma/\partial z)} \frac{\partial^2 K_\gamma}{\partial U_\alpha \partial z} \right], \tag{28}$$

$$B'_{\beta\alpha} = f_\epsilon^\beta \left[\frac{\partial g_\epsilon^\beta}{\partial(\partial U_\alpha/\partial z)} + \frac{\partial g_\epsilon^\beta}{\partial(\partial K_\gamma/\partial z)} \frac{\partial K_\gamma}{\partial U_\alpha} \right], \tag{29}$$

$$C'_{\beta\alpha} = f_\epsilon^\beta \frac{\partial g_\epsilon^\beta}{\partial(\partial^2 U_\alpha/\partial z^2)}, \tag{30}$$

$$V_\beta' = -g_\epsilon^\beta f_\epsilon^\beta + A'_{\beta\alpha} U_\alpha + B'_{\beta\alpha}(\partial U_\alpha/\partial z) + C'_{\beta\alpha}(\partial^2 U_\alpha/\partial z^2). \tag{31}$$

In Eqs. (28) to (31) the superscript $n + 1$ and subscripts i and j are expressly implied. Defining $(\Delta z_+)_j = z_{j+1} - z_j$ and $(\Delta z_-)_j = z_j - z_{j-1}$, and introducing spatial difference equations, we obtain

$$(\bar{A})_{i,j}^{n+1} \mathbf{U}_{i,j}^{n+2} + (\bar{B})_{i,j}^{n+1} \mathbf{U}_{i,j+1}^{n+1} - (\bar{C})_{i,j}^{n+1} \mathbf{U}_{i,j-1}^{n+2} = \mathbf{V}_{i,j}^{n+1}, \tag{32}$$

with

$$A_{\beta\alpha} = A'_{\beta\alpha} + \frac{\Delta z_+ - \Delta z_-}{\Delta z_+ \Delta z_-} B'_{\beta\alpha} - \frac{2}{\Delta z_+ \Delta z_-} C'_{\beta\alpha}, \tag{33}$$

$$B_{\beta\alpha} = \frac{\Delta z_-}{\Delta z_+(\Delta z_- + \Delta z_+)} B'_{\beta\alpha} + \frac{2}{\Delta z_+(\Delta z_- + \Delta z_+)} C'_{\beta\alpha}, \tag{34}$$

$$C_{\beta\alpha} = \frac{\Delta z_+}{\Delta z_-(\Delta z_- + \Delta z_+)} B'_{\beta\alpha} - \frac{2}{\Delta z_-(\Delta z_- + \Delta z_+)} B'_{\beta\alpha}, \tag{35}$$

and

$$V_{\beta\alpha} = V'_{\beta\alpha}. \tag{36}$$

Equations (21) and (32) represent two complete sets of finite difference approximations to the original differential equations (12). Each approximation is of first order accuracy in Δt and second order accuracy in space for a uniform mesh (Δr and Δz do not have to be equal); for a nonuniform mesh, the approximations to the terms involving second spatial derivatives are to first order accuracy only. When the two approximations are used on alternate time steps, an overall approximation to (12) that is second order in both time and space is obtained if the mesh is uniform as in the Peaceman–Rachford method.

The computational difficulties resulting from a finite difference treatment of strong shock waves have long been recognized in computational hydrodynamics, and various authors have presented methods for eliminating them. The idea behind all methods is to introduce into the differential equations that are to be solved an enhanced numerical dissipative mechanism which limits the steepness of any gradients that occur and smooths out the transition region to a length greater than one mesh interval. The most quoted method is the von Neumann–Richtmyer [14] "artificial viscosity."

In the early two-fluid magnetohydrodynamic calculations, Hain *et al.* [1] used the von Neumann–Richtmyer artificial viscosity technique. However, the artificial viscous pressure heating was confined to only the ion energy equation, simulating the experimentally observed heating of ions in regions of strong shocks. In the calculations of this paper we used the "smoothing" method of Lapidus [15], which was first used in MHD calculations by Freeman and Lane [4]. The method essentially adds artificial diffusion to all partial differential equations to be solved, so that the equations take the form

$$(\partial \mathbf{U}/\partial t) + \mathbf{T} + \mathbf{T}_r' + \mathbf{T}_z' = 0, \tag{37}$$

where

$$\mathbf{T}_r' = -a^2(\Delta r)^2 \frac{\partial}{\partial r}\left(\left|\frac{\partial v_r}{\partial r}\right| \frac{\partial \mathbf{U}}{\partial r}\right)$$

$$\mathbf{T}_z' = -a^2(\Delta z)^2 \frac{\partial}{\partial z}\left(\left|\frac{\partial v_z}{\partial z}\right| \frac{\partial \mathbf{U}}{\partial z}\right)$$

where a is a constant of order unity. The use of Eq. (37) is appropriate only if the components of $\mathbf{U}$ are conserved quantities, e.g., mass, momentum, total energy, etc. When (37) is applied to a nonconservative form of the ion energy equation, an additional artificial viscous heating term should be included to account for the effective viscosity added to the equation of motion, and to assure conservation of energy. In the sample calculations given in this paper, this additional ion heating term was not included, however. Our most recent calculations use a von Neumann–Richtmyer artificial viscosity.

Several of the sets of magnetohydrodynamic equations which take into account anisotropy introduced by the magnetic field will involve mixed second partial derivatives, i.e., $\partial^2\mathbf{U}/\partial r\,\partial z$, in the partial differential equations to be solved. Mixed second partial derivatives are also introduced if an equation for the stream function ψ, defined in Eq. (10), is used to replace the equations for the radial and axial magnetic fields, B_r and B_z, respectively.

The solution of the sets of linear equations given by (21) or (32) is accomplished using the standard method [16] for tridiagonal systems. When mixed second partial derivatives are present the equations are differenced in such a way as to preserve the tridiagonal form of the equations and still retain the implicit form of the equations.

The method for treating the mixed derivatives is essentially that used by Marx [17] in the ADI numerical solution of the Fokker–Planck equation. The method results from successive Taylor approximations as follows:

$$\begin{aligned}\left(\frac{\partial^2\mathbf{U}}{\partial r\,\partial z}\right)_{i,j}^{n+1} &= \frac{1}{2}\left(\frac{\partial^2\mathbf{U}}{\partial r\,\partial z}\right)_{i,j+1/2}^{n+1} + \frac{1}{2}\left(\frac{\partial^2\mathbf{U}}{\partial r\,\partial z}\right)_{i,j-1/2}^{n+1} + 0[(\Delta z)^2] \\ &= \frac{1}{2}\left(\frac{\partial^2\mathbf{U}}{\partial r\,\partial z}\right)_{i,j+1/2}^{n} + \frac{\Delta t}{2}\left(\frac{\partial^3\mathbf{U}}{\partial r\,\partial z\,\partial t}\right)_{i,j}^{n+1} + 0[\Delta t\,\Delta z] + 0[(\Delta t)^2] \\ &\quad + \frac{1}{2}\left(\frac{\partial^2\mathbf{U}}{\partial r\,\partial z}\right)_{i,j-1/2}^{n+1} + 0[(\Delta z)^2] \end{aligned} \tag{38}$$

and

$$\begin{aligned}\left(\frac{\partial^2\mathbf{U}}{\partial r\,\partial z}\right)_{i,j}^{n+2} &= \frac{1}{2}\left(\frac{\partial^2\mathbf{U}}{\partial r\,\partial z}\right)_{i+1/2,j}^{n+2} + \frac{1}{2}\left(\frac{\partial^2\mathbf{U}}{\partial r\,\partial z}\right)_{i-1/2,j}^{n+2} + 0[(\Delta r)^2] \\ &= \frac{1}{2}\left(\frac{\partial^2\mathbf{U}}{\partial r\,\partial z}\right)_{i+1/2,j}^{n+1} + \frac{1}{2}\left(\frac{\partial^2\mathbf{U}}{\partial r\,\partial z}\right)_{i-1/2,j}^{n+2} + \frac{\Delta t}{2}\left(\frac{\partial^3\mathbf{U}}{\partial r\,\partial z\,\partial t}\right)_{i,j}^{n+2} \\ &\quad + 0[\Delta r\,\Delta t] + 0[(\Delta t)^2] + 0[(\Delta r)^2]. \end{aligned} \tag{39}$$

The final difference equations are obtained by retaining only the first and fifth terms on the right-hand side of the last equality in (38) and the first two terms on the right-hand side of the last equality in (39) and approximating the retained terms correct to second order (for a uniform mesh; for a nonuniform mesh, the analogous

approximations will be first order only, just as for the nonmixed second partial derivatives). The final difference equations corresponding to (38) and (39) are, respectively,

$$\left(\frac{\partial^2 \mathbf{U}}{\partial r\,\partial z}\right)_{i,j}^{n+1} = \frac{1}{4\Delta r\,\Delta z}\left[\mathbf{U}_{i+1,j}^{n+1} - \mathbf{U}_{i-1,j}^{n+1} - \mathbf{U}_{i+1,j-1}^{n+1} + \mathbf{U}_{i-1,j-1}^{n+1}\right.$$
$$\left. + \mathbf{U}_{i+1,j+1}^{n} - \mathbf{U}_{i-1,j+1}^{n} - \mathbf{U}_{i+1,j}^{n} + \mathbf{U}_{i-1,j}^{n}\right], \tag{40}$$

$$\left(\frac{\partial^2 \mathbf{U}}{\partial r\,\partial z}\right)_{i,j}^{n+2} = \frac{1}{4\Delta r\,\Delta z}\left[\mathbf{U}_{i,j+1}^{n+2} - \mathbf{U}_{i,j-1}^{n+2} - \mathbf{U}_{i-1,j+1}^{n+2} + \mathbf{U}_{i-1,j-1}^{n+2}\right.$$
$$\left. + \mathbf{U}_{i+1,j+1}^{n+1} - \mathbf{U}_{i+1,j-1}^{n+1} - \mathbf{U}_{i,j+1}^{n+1} + \mathbf{U}_{i,j-1}^{n+1}\right]. \tag{41}$$

Equations (40) and (41) assume an ascending sequence of j and i, respectively, in the solution of (21) and (32). Thus the first two terms on the right-hand side of Eqs. (40) and (41) give contributions to the matrices $\bar{B}$ and $\bar{C}$ of Eqs. (21) and (32), and the remaining quantities—although some are "implicit," they are known—give contributions to the vectors V. Getting started, i.e., calculating at $j = 2$ for the first time step and at $i = 2$ for the second, can be accomplished by using the boundary conditions.

The overall two-step truncation error of (40) and (41) is

$$e = O[(\Delta t)^2] + O[(\Delta r)^2] + O[(\Delta z)^2] + O[\Delta r\,\Delta t] + O[\Delta z\,\Delta t]$$

for a uniform mesh.

The basic method outlined above is applicable to the partial differential equations written so that all derivatives are completely expanded, i.e., so that the equations indeed have the functional form indicated by Eq. (14). In the basic method, terms of each equation are then broken into two parts, and one part is treated implicitly on the first time step and the second part is treated implicitly on the second time step. Nonlinear terms in the implicitly treated part are linearized in time.

Alternating direction implicit finite difference equations can also be derived [18] for the equations written in "conservation" form [2]. Again, the terms in the equations are broken into two parts, one containing all r derivatives and one containing all z derivatives, and the former part is treated implicitly on the first time step and the latter on the second.

Application: Theta Pinch

In this section the ADI methods developed are applied to the problem of following the dynamics of a two-dimensional theta pinch. As has been mentioned previously, nearly all significant magnetohydrodynamic computational research

has been concerned with stabilized z and theta pinches. Consequently, application of numerical techniques to the study of the theta pinch is not a new idea. However, the inclusion of tensor thermal conductivities in the differential equations and the use of ADI numerical techniques are both features which were not used in previously reported two-dimensional calculations.

The equations used for the calculations reported in this section are a subset of two-fluid MHD equations. The vector to be calculated is

$$\mathbf{U} = (\rho, v_r, v_z, \theta_i, \theta_e, B_r, B_z), \tag{42}$$

and the transport coefficients involved in the equations are

$$K = (K_i^{rr}, K_i^{rz}, K_i^{zz}, K_e^{rr}, K_e^{rz}, K_e^{zz}, f_{eq}, \eta_{\varnothing\varnothing}). \tag{43}$$

Azimuthal magnetic fields are excluded by definition, so if the plasma azimuthal motion is initially zero it will remain so; hence the exclusion, also, of $v_\varnothing$.

For the applications, the transport coefficients and their derivatives have not been treated implicitly, i.e., in (15) and (26) $\partial K_\gamma/\partial U_\alpha = 0$. When the code was originally developed, scalar transport coefficients were used, and the implicit methods were implemented rigorously. When the matrix transport coefficients were incorporated, they were treated explicitly. Since the transport coefficients and their spatial derivatives are not treated implicitly, the truncation error of those terms in which transport coefficients appear reverts to first order in Δt.

The calculations to be presented in this section are not an attempt to model a real device. They are rather intended to display the basic physical features of the pinch and to suggest the use of the ADI method for future calculations attempting to correlate with experiment. Therefore, the region of solution is taken to be the rectangular region depicted in Fig. 1. For the calculations reported in this paper the domain of solution is subdivided into a 30×40 mesh, 30 points in the radial direction and 40 in the axial direction. The grid points are equally spaced in the radial and axial directions. To permit proper centering of the boundary conditions, no points lie on the boundaries $\overline{OA}$, $\overline{AB}$, and $\overline{OC}$. These boundaries are taken to lie halfway between the boundary rows of points and the first interior rows. The boundary $\overline{BC}$ coincides with the outermost axial row of points.

The theta pinch gas is assumed to be fully ionized and initially uniform and at rest in a cylindrical region 4 cm in diameter with 7 cm between mirrors; because of symmetry it is sufficient to calculate the variables in a domain 2 cm $\times$ 3.5 cm in the r–z plane. The initial plasma density is 6.9×10^{15} ions/cm^3 and the temperature is 5 eV. The plasma had imbedded in it an initial homogeneous forward bias field of 2 kilogauss. A 100 kilogauss magnetic field with mirror ratio of 2 and sinusoidal rise time of 2.5 μsec is applied at zero time.

Symmetry boundary conditions are used at the plane and axis of symmetry.

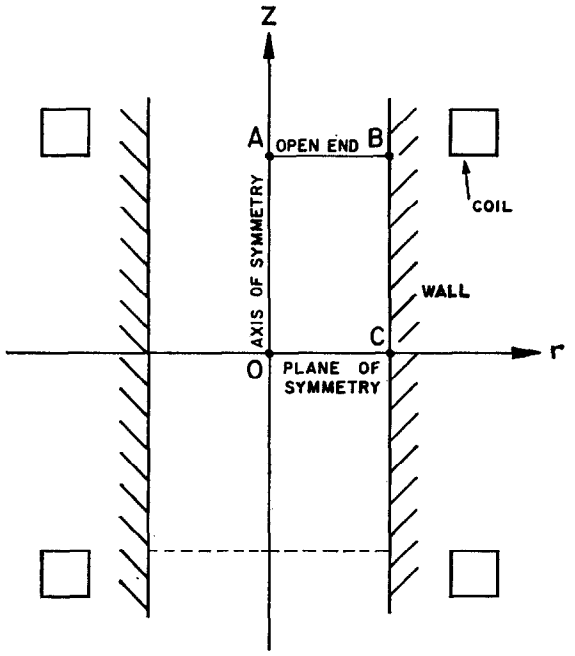

FIG. 1. Theta pinch region of solution.

Values of all quantities except the radial magnetic field at the first interior point are reproduced on the mirror boundary; the radial magnetic field is set to zero so that the field lines are axial at the mirror. At the "wall" the magnetic field is specified and all fluid quantities are treated similarly to the method of Hain *et al.* [1] and Roberts *et al.* [2], who have discussed in detail the problem at the boundary; hence, a low density background gas is continually created at the wall as the main plasma implodes.

Figures 2 through 4 show the initial implosion and subsequent rebound, or "bounce." In the figures, the axis of symmetry is to the left, the plane of symmetry to the front, the wall to the right, and the mirror to the rear; the plasma density values at the actual finite grid points are plotted, although the scale in each figure is different and the zero is essentially the value at the wall and not the bottom of the figure. Because of the mirror field, the plasma in the mirror region is accelerated more rapidly than that at the plane of symmetry (Fig. 2) and is the first to converge on the axis and rebound (Fig. 3). As the mirror plasma rebounds the plasma at the plane of symmetry converges on the axis (Fig. 4).

High compression occurs in the mirror region because of the strong fields, but the highest compression ($1.6 \times 10^{17}/\text{cm}^3$) occurs at the plane of symmetry because

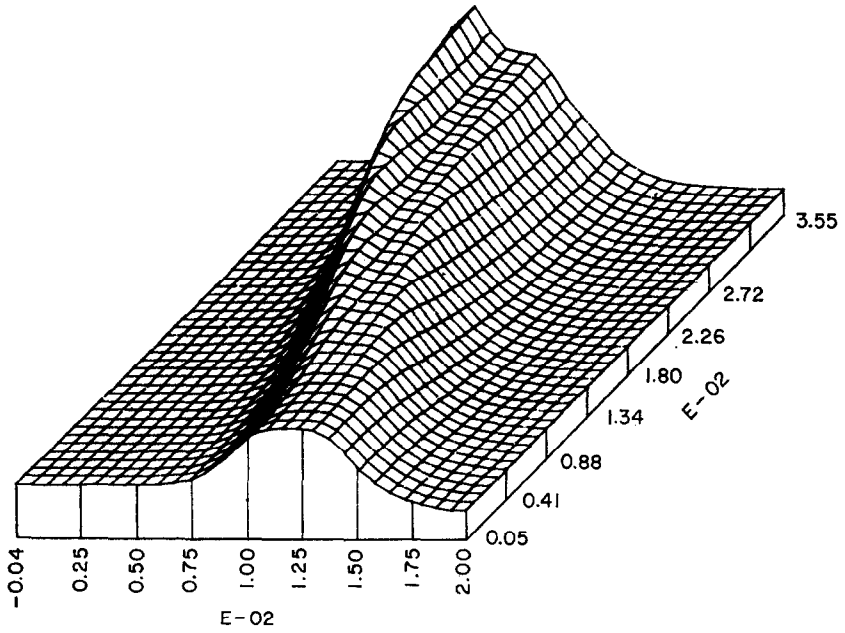

FIG. 2. Theta pinch density at 0.2 μsec. $(n_i)_{max} \approx 4.1 \times 10^{16}/cm^3$.

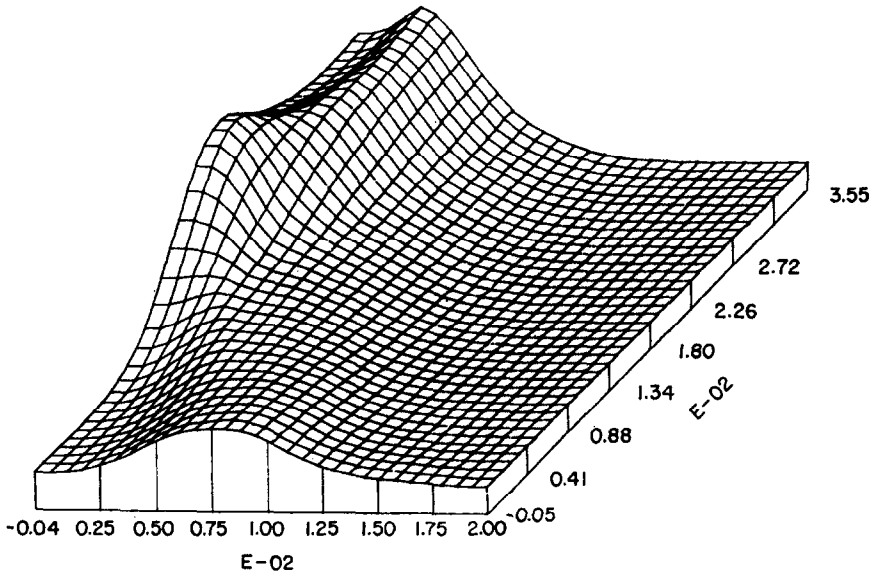

FIG. 3. Theta pinch density at 0.2506 μsec. $(n_i)_{max} \approx 1.1 \times 10^{17}/cm^3$.

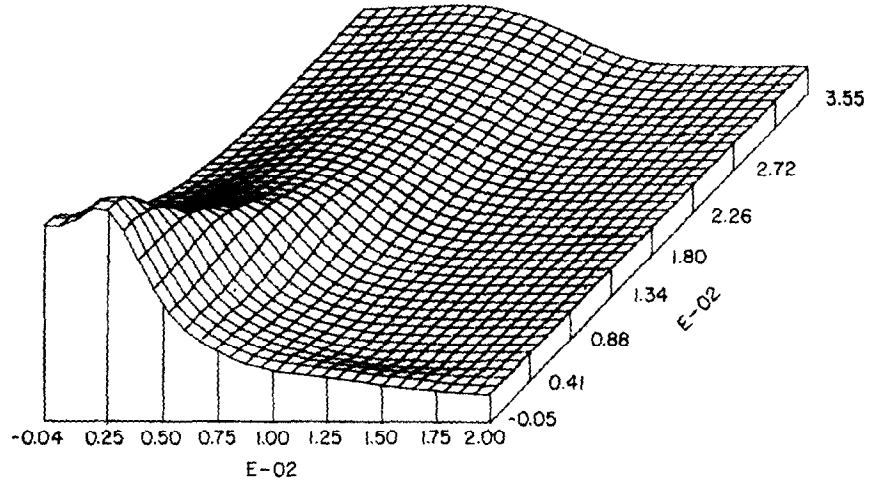

FIG. 4. Theta pinch density at 0.3019 μsec.

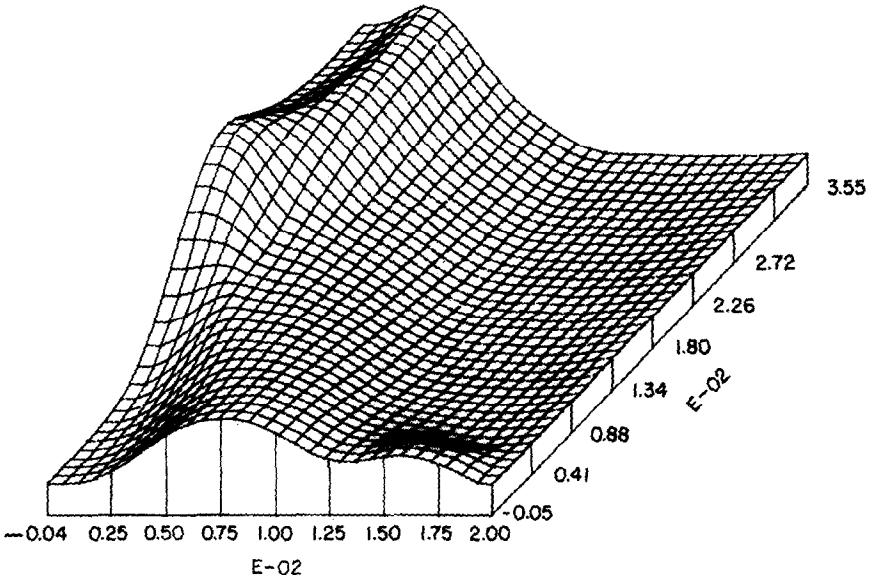

FIG. 5. Theta pinch ion temperature at 0.2506 μsec. $(T_i)_{max} \approx 34$ eV.

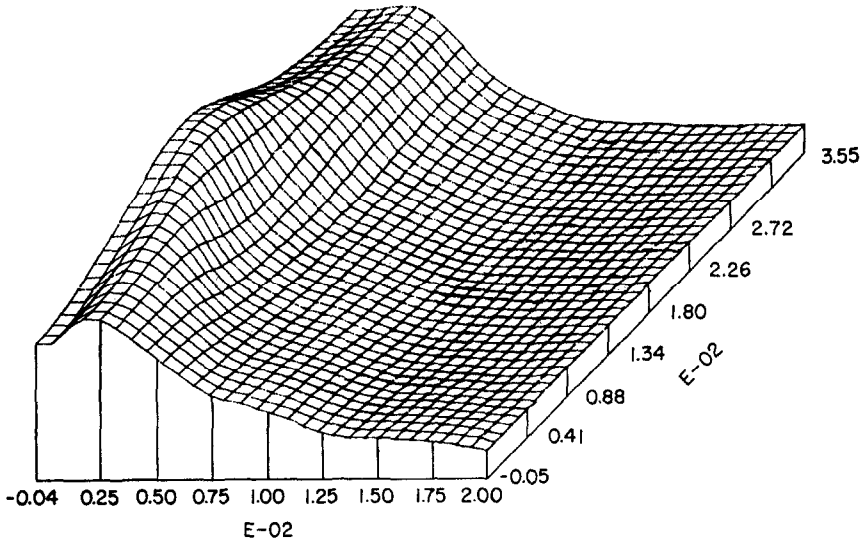

FIG. 6. Theta pinch electron temperature at 0.2506 μsec. $(T_e)_{max} \approx 57$ eV.

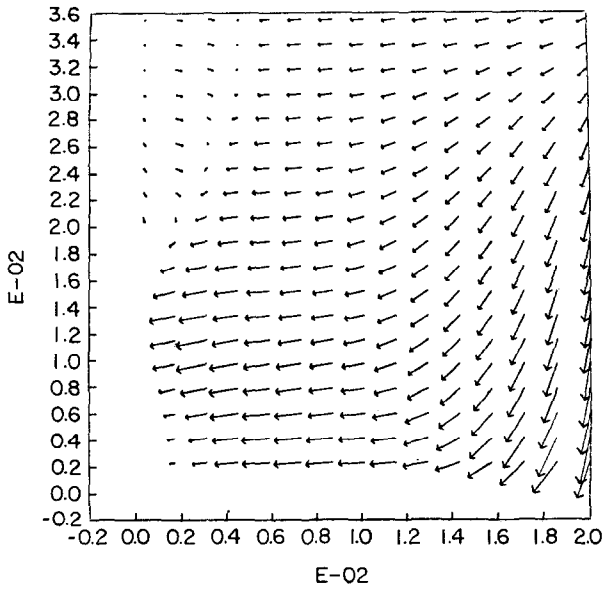

FIG. 7. Theta pinch flow field at 0.2506 μsec.

of axial motion of the plasma toward that plane. The ion temperature follows from the approximately adiabatic compression of the ions and indicates little energy gain from the hot electrons. The electron temperature is a result of resistive heating, adiabatic compression, and thermal conduction along magnetic field lines. Figures 5 and 6 show the ion and electrons temperature profiles corresponding to Fig. 3. It is to be noted that although very little compression and resistive heating has occurred at the plane of symmetry near the axis, the electron temperature is very much higher than the initial temperature. The reason is the strong thermal conduction to this region along field lines from regions of strong compression and heating. Hence, thermal conduction is a preheat mechanism for plasma at the center of the plasma, and the values of thermal conductivity involved suggest that this can be an important effect in considerably longer systems.

Figure 7 shows the motion of the plasma corresponding to Fig. 3. Although the motion of the imploding plasma is primarily radial, all plasma has some negative axial motion, and a large part of the rebounding plasma's motion is axial (upper left corner of Fig. 7). An examination of the forces causing the axial motion shows that it is primarily the axial pressure gradients resulting from the more rapid radial implosion of the plasma near the mirror, and not the magnetic field curvature, which axially accelerates the plasma. This conclusion agrees with the experimental observations of Sato *et al.* [19]. The motion of the rebounding plasma and the motion at the start of the reimplosion suggests that on the second pinch the axial flow will be considerably greater than during the initial implosion.

Application: Laser-Produced Plasma

Theoretical consideration of the dynamics of the expanding plasma produced by laser irradiation has been confined to one-dimensional spherical models. Dawson [20] derived an integrated similarity model, assuming uniform density and temperature and a radial velocity that increases linearly from the center to the edge, and was able to predict features of the plasma motion in the absence of a magnetic field. Fader [21] used finite difference techniques to solve directly the one-dimensional (spherical), single-fluid, hydrodynamic partial differential equations, including absorption of energy from the laser beam. Kidder [22] obtained numerical solutions to the one-dimensional, two-fluid hydrodynamic equations. Nuckolls *et al.* [23] have discussed the possibilities of thermonuclear reactions in laser-irradiated pellets.

Attempts to describe the interactions of the plasma and a confining magnetic field have also been limited primarily to one-dimensional models. Bhadra [24] has extended Dawson's model to include a magnetic field and resistive effects and has illustrated qualitatively some features of the "bouncing" of the plasma against

the field. Fader *et al.* [25] have incorporated the magnetic field into the one-dimensional hydrodynamic equations and have solved the equations numerically. McKee [26] has used Bhadra's magnetic field treatment in a spherical integrated similarity model which assumes a density profile that decreases linearly with radius. Poukey [27] has done a two-dimensional calculation of the motion of an infinite-conducting plasma shell in an initially homogeneous magnetic field.

It is the purpose of this section to apply the two-fluid MHD model and the ADI numerical methods to the study of the trapping and thermalization of a high-density, high-temperature, i.e., laser-produced, plasma expanding into a magnetic field. The calculations will use as initial conditions results obtained by others in

[redacted] the plasma-field interaction.

It is convenient in the Eulerian approach to solving MHD equations to have a background plasma present throughout the region of solution, so that plasma equations can be used. The alternate choice, plasma equations at some points and vacuum equations at others, has been discussed by Roberts and Potter [2]. The appropriate vacuum equation is elliptic, but efficient methods are available for solving the elliptic equation. A major difficulty in using the alternate approach for the problem considered here appears to be the determination of the plasma-vacuum interface on a finite orthogonal mesh. The more convenient approach, background plasma everywhere, has been chosen for our calculations.

The set of magnetohydrodynamic equations appropriate for study of the expanding laser-produced plasma is the same set of equations appropriate for the study of the theta pinch. However, the ion pressure P_i, the electron pressure P_e, and the plasma magnetic stream function ψ^P were chosen to be dependent variables. The magnetic field stream function is separated into plasma and external components, i.e.,

$$\psi^T = \psi^P + \psi^E, \tag{44}$$

where

$$\frac{\partial^2 \psi^E}{\partial r^2} + \frac{\partial^2 \psi^E}{\partial z^2} - \frac{1}{r}\frac{\partial \psi^E}{\partial r} = 0. \tag{45}$$

Therefore, the vector to be calculated is

$$\mathbf{U} = (\rho, v_r, v_z, P_i, P_e, \psi^P), \tag{46}$$

and the transport coefficients appearing in the differential equations are

$$\mathbf{K} = (K_i^{rr}, K_i^{rz}, K_i^{zz}, K_e^{rr}, K_e^{rz}, K_e^{zz}, f_{eq}, \eta_{\varnothing\varnothing}). \tag{47}$$

The two pressures have been chosen because in the course of the expansion the

temperatures in the interior region of the main plasma become less than the temperatures in the outer region, even though the pressures are greater in the interior. Consequently the plasma motion is from a region of lesser temperature into a region of higher temperature, and calculations using the temperatures as dependent variables eventually yield nonphysical low and negative temperatures which could only be prevented by using the one-sided, first-order finite difference approximations to the first spatial derivative. By contrast, plasma motion is from a region of higher to lower pressure for a longer time, so with pressures as dependent variables fewer difficulties arise with the use of the standard space-centered second-order finite difference approximations to the first spatial derivatives.

The difference method used is essentially the method described earlier. The transport coefficients and their derivatives are treated explicitly. A major difference between the method described and the actual difference equations used is in the treatment of the thermal conduction terms in the pressure equations. All thermal diffusion terms are written in flux-divergence form rather than in completely expanded form.

The initial conditions for the calculations are taken from numerical results obtained by McKee [26]. McKee's calculations are for a quartz fiber irradiated by a 117 megawatt, 25 nanosecond neodymium laser, thus creating a plasma of 7.5×10^{15} ions; the quartz fiber is placed in an initially homogeneous 10 kG magnetic field. McKee's calculations show that at 25 nsec after the laser beam is initiated, the plasma has expanded to a radius of 0.1 cm and has a uniform (by assumption) temperature of 10 eV; the corresponding skin depth is approximately 0.04 cm, indicating that the magnetic field has been excluded from the plasma, and the plasma boundary radial velocity is 1.01×10^7 cm/sec.

The plasma will be assumed to be initially spherically symmetric, so initial conditions can be described in terms of the spherical radius, $R = (r^2 + z^2)^{1/2}$. The initial density and temperature will be taken to decrease linearly from a maximum at the origin to some minimum at a radius $R = R_0$. The initial spherical radial velocity of the main plasma will be taken to increase linearly to a maximum at radius R_0. If the background plasma, i.e., the plasma outside R_0, is initially stationary, the numerical solutions obtained will depend very strongly on the adiabatic shock speed (or, equivalently, the temperature) of the background plasma and will not closely approximate the solution which would be obtained if a vacuum were present. Consequently, the background plasma will also be initially in motion with a velocity profile having a maximum at R_0 and decreasing linearly to zero at some multiple of R_0. The magnetic field will be initially uniform and directed in the z direction. It follows that the initial total stream function ψ^T must be parabolic in r and independent of z, and because the magnetic field is uniform, the plasma stream function ψ^P is initially zero.

The initial plasma radius R_0 is taken to be 0.1 cm and the velocity at R_0 is

10^5 m/sec. The uniform axial magnetic field is 10 kG. The density and temperature at the origin are 7.2×10^{18} ions/cm^3 and 25 eV, respectively. Straightforward calculations show that the plasma described contains, within a sphere of radius R_0 centered at the origin, 7.5×10^{15} ions having a kinetic energy of about 0.5 J (joule) and a total thermal energy of 0.036 J. Except for the different temperature profile, the initial main plasma is in the same configuration as McKee's plasma 25 nsec after the initiation of laser irradiation. Although McKee's calculations indicate that by 25 nsec the magnetic field is excluded from the plasma, the initial field for our calculations is taken to be uniform everywhere, including the main plasma, since it is impossible to resolve differences over length scales comparable to the skin depth of McKee's calculations on a finite mesh of the size indicated below. The total mass in the background plasma is about one-third of the mass of the main plasma. However, the total kinetic energy of the background plasma is less than 0.01 J and the thermal energy less than 1.5×10^{-4} J, which should be compared to the magnetic field energy of 6.25 J. Therefore, it is conjectured that the existence of the background plasma, because of its initial motion and because of its low energy density, should not seriously affect the dynamics of the main plasma.

The region of solution is taken to be the rectangular region in the r–z plane shown in Fig. 8. As for theta pinch calculations, $\overline{OC}$ and $\overline{AO}$ will be a plane and

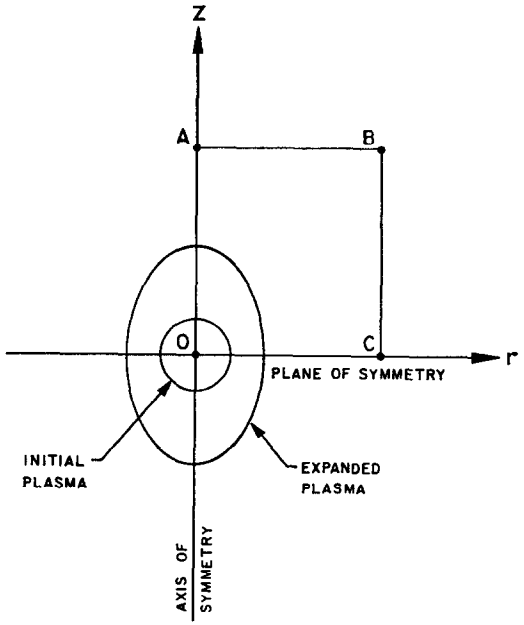

FIG. 8. Region of solution for laser-produced plasma.

axis, respectively, of symmetry, but $\overline{AB}$ and $\overline{BC}$ will be merely interpreted as being regions sufficiently far from the origin that boundary conditions applied at these boundaries do not greatly affect the calculations. The region of solution is broken up into a 33 by 37 mesh, 33 mesh points in the radial direction and 37 in the axial direction. For the first 20 mesh points in both direction, the point spacing is uniform and the same in both directions. For the remaining points the spacing is nonuniform, increasing geometrically with a common ratio of 1.065, and is slightly different in each direction. The uniform region in the center is used to give the calculations a chance to "settle down" before the main plasma enters the nonuniform mesh. As in the theta pinch case, the boundaries $\overline{OA}$, $\overline{AB}$, and $\overline{OC}$ are centered between the outermost rows of mesh points, and the boundary $\overline{BC}$ coincides with the outermost row.

The same boundary conditions as used for the theta pinch calculations of the previous section are imposed at the boundary $\overline{AB}$, so that the axial derivatives of all quantities are set to zero. On $\overline{BC}$, the density and temperatures, and hence pressures, are held at their initial values, and the normal, i.e., radial, derivatives of all other quantities are set to zero. Setting the radial derivative of ψ^P to zero on $\overline{BC}$ is equivalent to requiring the total axial field at that boundary to remain unchanged; however, it does allow magnetic flux to pass out of the boundary.

The boundary conditions which have been discussed are quite simple from both a physical and a computational standpoint. The simplicity on boundaries $\overline{OA}$ and $\overline{OC}$ results, of course, from the assumed symmetry and is therefore physically correct. On the other hand, the boundary conditions imposed on $\overline{AB}$ and $\overline{BC}$ can only be correct if indeed these boundaries are located far from the main plasma.

We wish to explain the formation of the high temperature shell observed in experiments and to predict a "bounce" radius at which the expanding motion transverse to the magnetic field is stopped. As the laser-produced plasma moves across the magnetic field, azimuthal currents are induced in the plasma. As demonstrated by the various one-dimensional models, the currents are localized in the outer regions of the plasma and it is the interaction of the induced currents with that magnetic field which eventually halts the transverse motion of the plasma.

As the plasma expands, it takes on a nonspherical shape. The plasma density shows some deviation from spherical symmetry at 26.1 nsec as is shown in Fig. 9. The electron pressure profile at 26.1 nsec is shown in Fig. 10. A shell of very high pressure and high temperature has formed at much of the main plasma boundary. This shell is a result of the very localized currents at the boundary due to transverse motion across the magnetic field. The location of the currents is shown in Fig. 11. Because of the extremely high electron parallel thermal conductivity due to the high temperatures, thermal equilibrium between the main plasma and the background plasma is established along magnetic field lines. The corresponding heat

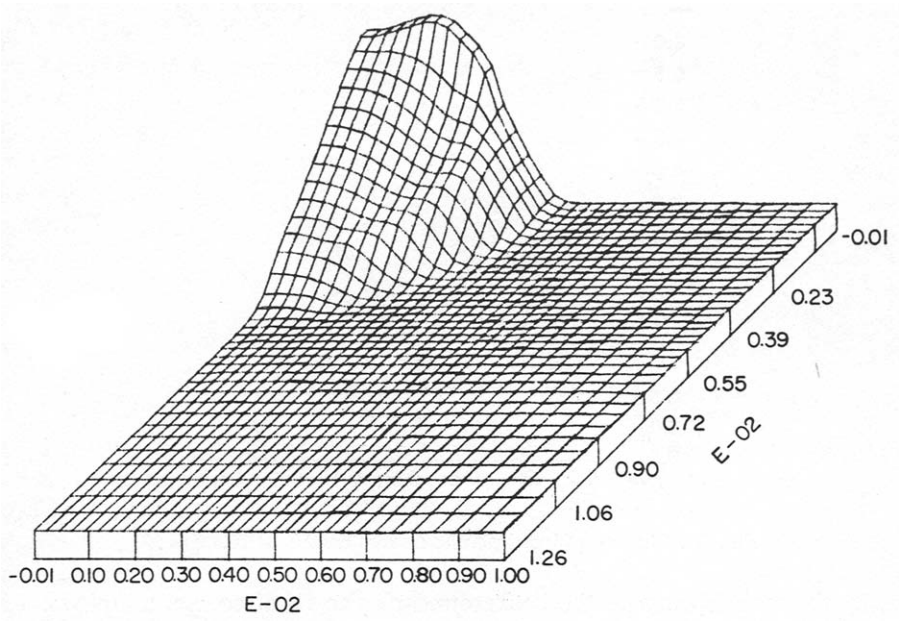

FIG. 9. Laser-produced plasma density at 26.1 nsec. $(n_i)_{max} \approx 1.8 \times 10^{17}/cm^3$.

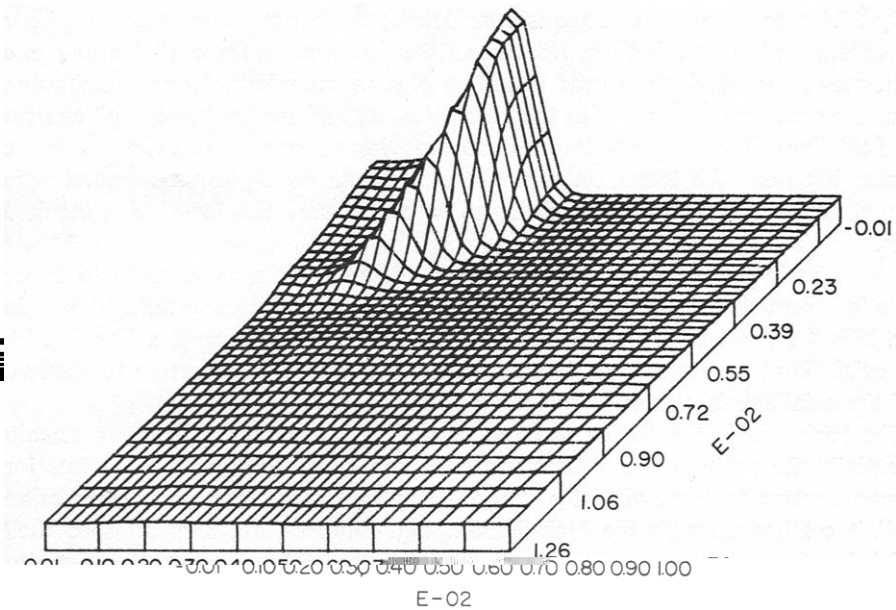

FIG. 10. Laser-produced plasma electron pressure at 26.1 nsec.

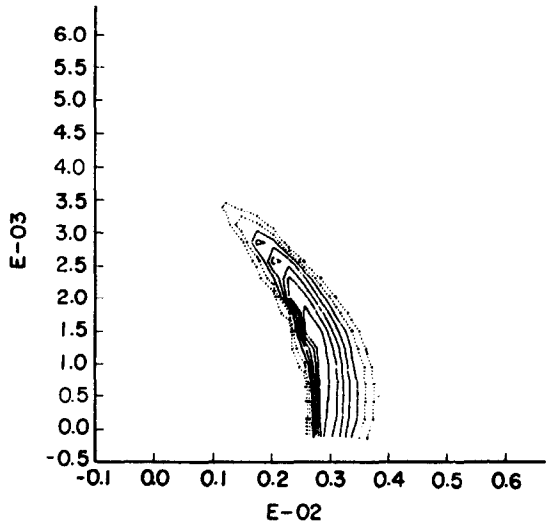

FIG. 11. Laser-produced plasma current density at 26.1 nsec.

loss by the main plasma to the background plasma is, of course, nonphysical if a true vacuum is being modeled, but because of the low density, and hence low specific heat, of the background, little energy is involved.

By 57.6 nsec the plasma shape is considerably aspherical. Shown in Fig. 12 is the density profile at this time. Because of the decelerating force of the magnetic field, plasma is decelerated near the main plasma boundary. Plasma expanding from the center catches up with the outer plasma, and matter "piles up" against the field lines. The interior plasma is still moving spherically outward from the origin; but near the interface, where the magnetic field-plasma interaction is strong, the plasma motion is beginning to be bent toward the direction of the field lines.

As the main plasma expands there is a tendency for the magnetic field to be excluded from the plasma; i.e., total magnetic flux is nearly constant. Shown in Fig. 13 is the total axial magnetic field, $B_z^T(B_z^T = B_z^P + B_z^E)$, profile. For Fig. 13, the origin is at the lower right-hand side, the radial axis is increasing to the left, and the axial axis is increasing to the right rear.

The basic qualitative features of the expanding laser-produced plasma remain essentially the same as the plasma moves outward and "bounces." The interior plasma appears to move virtually unaffected by the outer plasma-field interaction until it catches up with the high-density, high-temperature, high-pressure shell which has formed because of the deceleration of the plasma motion transverse to the magnetic field. The shell structure is most pronounced at the plane of symmetry, where all motion is transverse motion, and the structure becomes less pronounced

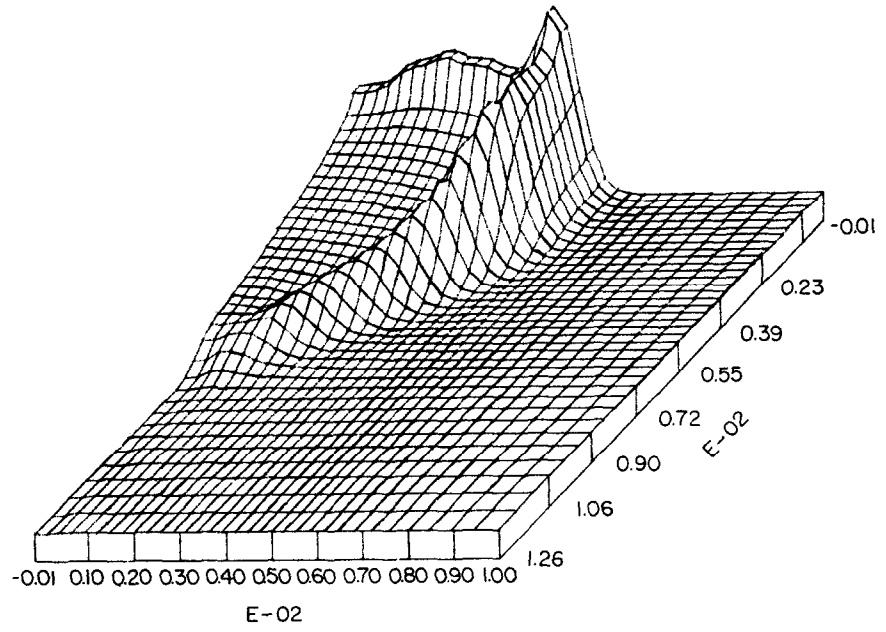

FIG. 12. Laser-produced plasma density at 57.6 nsec. $(n_i)_{max} \approx 3.3 \times 10^{16}/cm^3$.

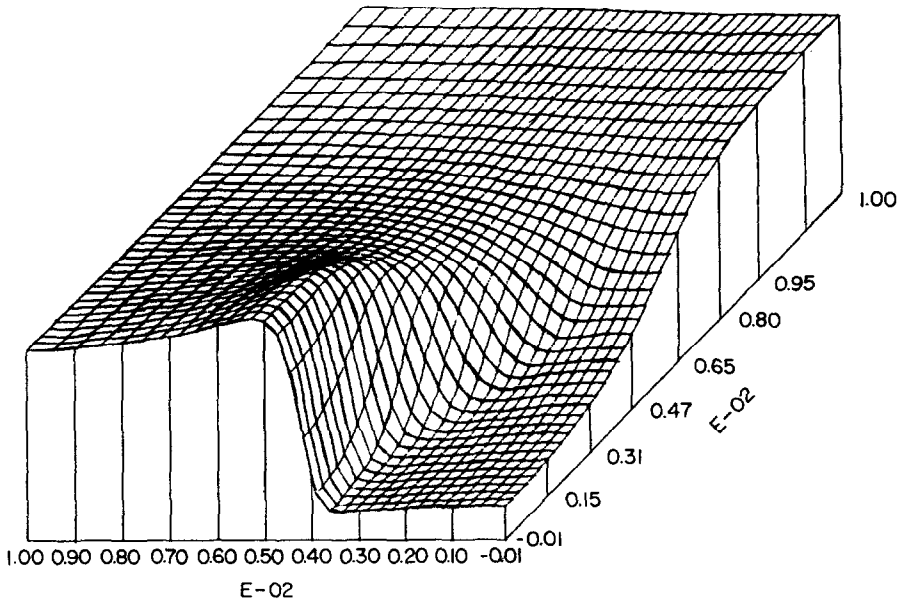

FIG. 13. Laser-produced plasma total axial magnetic field at 57.6 nsec.

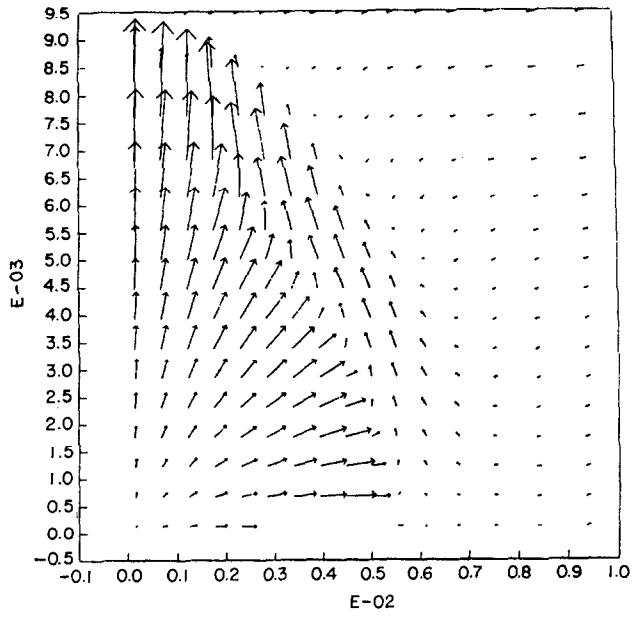

FIG. 14. Laser-produced plasma flow field at 113.5 nsec.

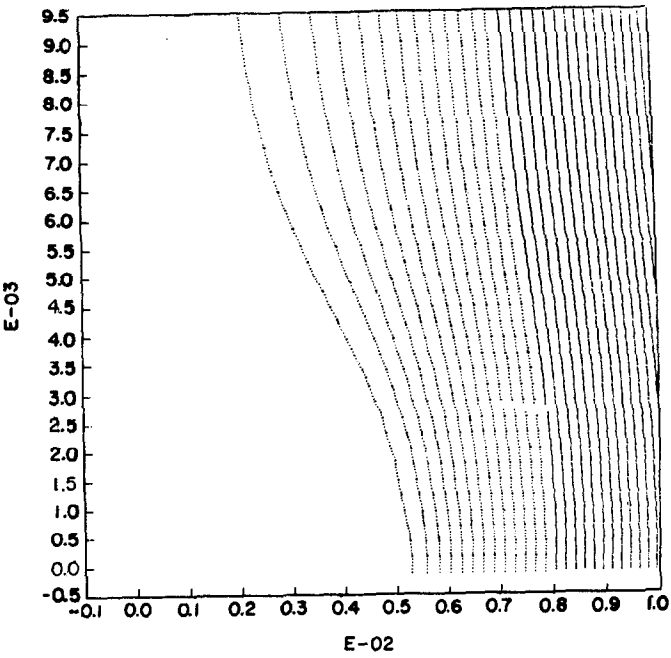

FIG. 15. Laser-produced plasma total stream function at 113.5 nsec.

away from the plane of symmetry where the plasma motion is oblique to the field lines. The motion of the obliquely moving plasma in the shell is bent in the direction of the field. The axial component, as well as the radial component, of the motion is decreased as the plasma forms its own mirror.

By $t = 113.5$ nsec much of the shell has a negative radial velocity (Fig. 14); however, the plasma motion with respect to the magnetic field is still mostly outward as the field lines in Fig. 15 indicate. Only near the plane of symmetry has the transverse motion actually stopped and reversed. The bounce radius is about 0.6 cm. To what extent the remainder of the plasma will bounce in the mirror field it creates has not yet been investigated.

These laser-produced plasma calculations show the formation of a high-density ($n_i > 10^{16}/\text{cm}^3$) shell at the outer region of the expanding plasma. The high density is a result of the deceleration of the plasma by the magnetic field. The calculations indicate that electron thermal equilibrium is established along magnetic field lines. The magnetic field is strong enough, however, to inhibit thermal conduction across the field lines, and hence the high temperature persists. The formation and persistence of a luminous shell as a laser-produced plasma expands against a magnetic field has been observed in the experiment of Tuckfield and Schwirzke [28] and the calculations presented here suggest that the shell can be explained from a purely classical standpoint.

Numerical Stability Criteria

When a set of nonlinear partial differential equations such as those discussed are solved numerically, the stability analysis of the corresponding difference scheme is very difficult. Consequently, a stability analysis of the alternating-direction implicit difference equations is beyond the scope of this paper. It is expected that the implicit techniques will allow calculations to be performed with a larger time step Δt than would be possible with explicit methods, i.e., enhanced numerical stability is expected.

We introduce the following numbers

$$S_1 = 2\frac{\Delta t}{\rho}\left[\frac{K_i^{rr}}{(\Delta r)^2} + \frac{K_i^{zz}}{(\Delta z)^2}\right], \tag{48}$$

$$S_2 = 2\frac{\Delta t}{\rho}\left[\frac{K_e^{rr}}{(\Delta r)^2} + \frac{K_e^{zz}}{(\Delta z)^2}\right], \tag{49}$$

$$S_3 = 2\frac{\Delta t \eta_{\phi\phi}}{\mu}\left[\frac{1}{(\Delta r)^2} + \frac{1}{(\Delta z)^2}\right], \tag{50}$$

$$S_4 = 2\frac{\Delta t}{\mu_0}\left[\frac{\eta_{rr}}{(\Delta r)^2} + \frac{\eta_{zz}}{(\Delta z)^2}\right], \tag{51}$$

$$S_5 = \frac{\Delta t}{\Delta r}\left[|\, v_r \,| + \left(\gamma\theta_i + \gamma\theta_e + \frac{B_z^2 + B_\varnothing^2}{\mu_0\rho}\right)^{1/2}\right], \tag{52}$$

$$S_6 = \frac{\Delta t}{\Delta z}\left[|\, v_z \,| + \left(\gamma\theta_i + \gamma\theta_e + \frac{B_r^2 + B_\varnothing^2}{\mu_0\rho}\right)^{1/2}\right], \tag{53}$$

$$S_7 = \Delta t f_{eq}\,. \tag{54}$$

It is conjectured that in the explicit numerical solution of the two-fluid MHD equations, the time step used would have to be small enough so that all of the numbers defined above would have to be less than or equal to unity at all mesh points as a necessary condition for numerical stability [29, 30]. The number S_2 is associated with electron thermal diffusion, S_3 is associated with resistive diffusion of the magnetic field, and S_5 is associated with magnetoacoustic waves. Figure 16 shows values of maximum S_2 and S_5 as a function of time for the theta pinch calculations; the discontinuities indicate changes in time step size. For the laser plasma calculations, the maximum S_2 was in general between 7.5 and 15.0, and the maximum S_3 was over 24. Thus, as expected, the alternating direction implicit finite difference equations permit a larger time step than explicit methods. For

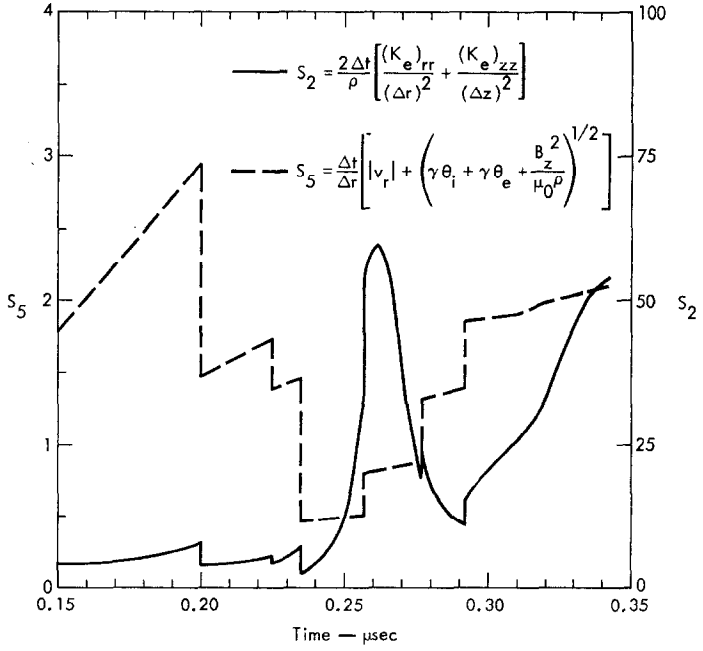

FIG. 16. Theta pinch stability numbers.

both calculations, the time step limitation was attributed to the mixed second derivative in the electron thermal conduction terms. In early laser-produced calculations using scalar transport coefficients, it was possible to operate with time steps such that S_2 was well over 100. Calculations have also been performed in parameter ranges where resistive and thermal diffusion was small, and in these instances, a maximum S_5 of over 40 was attained, and in near equilibrium states considerably higher values of S_5 have been attained.

Although no direct comparison has been made, we have argued [18] that the computer operating time per time step for a fully explicit code using the same model and doing the same problem should be no less than 20 % of the time required per time step for the code in which the alternating direction implicit methods of this paper have been implemented. Therefore, the calculations of this paper have been performed with less total computer operating time than might be required with a less sophisticated numerical method.

ACKNOWLEDGMENTS

This work was performed under the auspices of the U. S. Atomic Energy Commission. One of the authors (I. L.) would like to acknowledge the generous support of the Fannie and John Hertz Foundation.

REFERENCES

1. K. HAIN, G. HAIN, K. V. ROBERTS, S. J. ROBERTS, AND W. KOPPENDORFER, *Z. Naturforsch. A* **15** (1960), 1039.
2. K. V. ROBERTS AND D. E. POTTER, Magnetohydrodynamic calculations, in "Methods in Computational Physics" (B. Alder, S. Fernbach, and M. Rotenberg, Eds.), Vol. 9, p. 339, Academic Press, New York, 1970.
3. D. DUCHS, *Phys. Fluids* **11** (1968), 2010.
4. J. R. FREEMAN AND F. O. LANE, Initial Results from a Two-Dimensional Lax-Wendroff Hydromagnetic Code, Los Alamos Scientific Laboratory Report LA-3990 (1968), Proceedings of the 2nd Conference on Numerical Simulation of Plasmas, p. 278.
5. J. R. Freeman, *Nucl. Fusion* **11** (1971), 425.
6. D. E. POTTER, Numerical Studies of Two-Dimensional Magnetohydrodynamic Initial-Value Problems with Particular Application to Plasma Focus, Ph.D. Thesis, University of London (1970).
7. F. HERTWECK AND W. SCHNEIDER, "Proceedings of 2nd European Conference on Nuclear Fusion and Plasma Physics, Stockholm, 1967," p. 455.
8. W. SCHNEIDER, *Z. Physik*, **252** (1972), 147.
9. J. B. CHASE, J. L. LE BLANC, AND J. R. WILSON, Lawrence Livermore Laboratory Report UCRL-73014 Preprint, 1972, Accepted for publication in Phys. Fluids.
10. S. I. BRAGINSKII, Transport Processes in a Plasma, in "Reviews of Plasma Physics" (M. A. Leontovich, Ed.), Vol. I, p. 205, Consultants Bureau, New York, 1965.

11. D. W. PEACEMAN AND H. H. RACHFORD, JR., *J. Soc. Ind. Appl. Math.* **3** (1955), 28.
12. L. SPITZER, "Physics of Fully Ionized Gases," Interscience, New York, 1962, 2nd edition.
13. A. N. KAUFMAN, Plasma transport theory, in "La Theorie des Gaz Neutres et Ionises" (S. DeWitt and J. F. Detoeuf, Ed.), p. 295, Wiley, New York, 1960.
14. J. VON NEUMANN AND R. D. RICHTMYER, *J. Appl. Phys.* **21** (1950), 232.
15. A. LAPIDUS, *J. Comp. Phys.* **2** (1967), 154.
16. R. D. RICHTMYER AND K. W. MORTON, "Difference Methods for Initial Value Problems," Interscience, New York, 1967, 2nd edition.
17. J. KILLEEN AND K. D. MARX, The solution of the Fokker–Planck equation for a mirror confined plasma, in "Methods in Computational Physics" (B. Alder, S. Fernbach, and M. Rotenberg, Eds.), Vol. 9, p. 422, Academic Press, New York, 1970.
18. I. R. LINDEMUTH, The Alternating-Direction Implicit Numerical Solution of Time-Dependent, Two-Dimensional, Two-Fluid Magnetohydrodynamic Equations, Ph.D. Thesis, Lawrence Livermore Laboratory Report UCRL-51103, 1971.
19. K. SATO, I. KAWAKAMI, S. SHIINA, AND H. OHNISHI, *J. Phys. Soc. Japan* **30** (1971), 846.
20. J. DAWSON, *Phys. Fluids* **7** (1964), 981.
21. W. J. FADER, *Phys. Fluids* **11** (1968), 2200.
22. R. E. KIDDER, *Nucl. Fusion* **8** (1968), 3.
23. J. H. NUCKOLLS, L. WOOD, A. R. THIESSEN, AND G. B. ZIMMERMAN, *Nature* **239** (1972), 139.
24. D. K. BHADRA, *Phys. Fluids* **11** (1968), 234.
25. H. F. HAUGHT, D. H. POLK, J. C. WOO, AND W. J. FADER, Production of Plasma for Thermonuclear Research, Semiannual Report NYO-3578–11.
26. L. MCKEE, U. S. Naval Postgraduate School, Monterey, CA, private communication, 1971.
27. J. W. POUKEY, *Phys. Fluids* **12** (1969), 1452.
28. R. G. TUCKFIELD AND F. SCHWIRZKE, *Plasma Phys.* **11** (1969), 11.
29. JOHN KILLEEN, Computational problems in plasma physics and controlled thermonuclear research, in "Physics of Hot Plasmas" (B. J. Rye and J. C. Taylor, Eds.) pp. 202–255, Oliver and Boyd, Edinburgh, 1970.
30. JOHN KILLEEN, Computational Problems in Magnetohydrodynamics, in "Proceedings of International Federation for Information Processing Congress 71, Ljubljana, Yugoslavia, August 23-27, 1971," pp. 1191-1205, North-Holland, Amsterdam, 1972.